



CHORUS

This is the accepted manuscript made available via CHORUS. The article has been published as:

Ferroelectric to paraelectric phase transition mechanism in poled PVDF-TrFE copolymer films

A. Pramanick, S. Misture, N. C. Osti, N. Jalarvo, S. O. Diallo, and E. Mamontov

Phys. Rev. B **96**, 174103 — Published 3 November 2017

DOI: [10.1103/PhysRevB.96.174103](https://doi.org/10.1103/PhysRevB.96.174103)

Ferroelectric to paraelectric phase transition mechanism in poled PVDF-TrFE copolymer films

A. Pramanick,^{1,a)} S. Misture,² N. C. Osti,³ N. Jalarvo,^{3,4} S. O. Diallo,^{3, b)} E. Mamontov³

¹Department of Materials Science and Engineering, City University of Hong Kong, Kowloon, Hong Kong

²Kazuo Inamori School of Engineering, Alfred University, Alfred, New York, United States of America

³Chemical and Engineering Materials Division, Oak Ridge National Laboratory, Oak Ridge, Tennessee, United States of America

⁴Juelich Center for Neutron Scattering (JCNS -1), Forschungszentrum Juelich, Juelich, Germany

a) apramani@cityu.edu.hk

b) Current address: Smiths Detection Inc., Edgewood, Maryland, United States of America

Abstract

Direct experimental insights into the structural and dynamical mechanisms for ferroelectric β to paraelectric α phase transition in a poled PVDF-TrFE copolymer is obtained from *in situ* X-ray diffraction and quasielastic neutron scattering measurements at high temperatures. It is observed that the β -to- α phase transition proceeds through two energetically distinct processes, which are identified here as the nucleation and growth of an intermediate γ phase with random skew linkages followed by a γ -to- α transition. The two energetically distinct microscopic processes can explain the stages of evolution for β -to- α phase transition observed from heat flow measurements.

Poly(vinylidene fluoride) (PVDF) and its copolymers have been of great interest since their discovery several decades ago, owing to their large ferroelectric, pyroelectric and piezoelectric properties.¹⁻⁶ In recent years, interest in these materials have intensified due to their potential applications in electromechanical sensors and actuators, microelectronics, energy harvesting, electrocaloric and energy storage devices.⁷⁻¹² Peculiarly, for a polymeric material, PVDF and its copolymers are known to exist in several crystallographic forms, the most common among which are the α , β and the γ phases.^{13,14} These phases are defined as per the different configurations of monomers along the long C-chain, such as α phase with trans-gauche-trans-gauche' (TG TG') configuration formed by $\sim\pm 60^\circ$ dihedral angle between the neighboring monomer units, β phase with the all-trans (all-T) configuration formed by $\sim 180^\circ$ dihedral angle between the neighboring monomer units and γ phase with a kinked arrangement of T₃GT₃G'. In addition, variation in stacking of polymer chains also lead to additional phases such as δ and ϵ . The α phase is non-polar, while the β and γ phases are polar in nature. The functional properties of PVDF and its copolymers are determined by the respective crystallographic phases and therefore an understanding of their formation and stability becomes important. While there exists an extensive literature on the phase transition mechanisms in oxide ferroelectrics,^{15,16} similar studies on polymer ferroelectrics are rather rare.

In this respect, several recent studies have focused on elucidating the energy pathways and microscopic mechanisms for transition from the non-polar α to the polar β phase in PVDF and its copolymers.¹⁷⁻²³ This aspect becomes important in order to obtain the polar β form through appropriate processing as well as to optimize

subsequent operation for enhanced functionalities under electric fields.^{21,24-26} It is noteworthy that an α - β transformation requires upward and downward intramolecular rotations of CH_2 and CF_2 monomers around the G and G' bonds, which although thermodynamically feasible, are energy intensive processes.^{20,23} Therefore, instead of a direct α -to- β transition, a complicated combination of torsional and rotational motions is followed through the formation of intermediate phases of γ and δ as well as creation of microstructural disorders.^{20,23} While most of the studies so far have focused on the α -to- β transition, the reverse transition of β -to- α is not well understood. It is also important to mention here that while recent theoretical studies have predicted the pathways for α - β transformation, the details for the same are yet to be experimentally confirmed. Towards this end, we used two experimental probes of choice, namely X-ray diffraction and Quasielastic Neutron Scattering (QENS) to directly investigate *in situ* the structural and dynamical phenomena operative during β -to- α transition in a PVDF copolymer. Elucidation of these details for β -to- α transition will be important for understanding and controlling the factors affecting the thermal stability of PVDF copolymers which directly impacts the electrocaloric and energy storage capabilities of these polymers.

Specifically, we have investigated the crystallographic and mesoscopic mechanisms for transition from the polar β to the non-polar α phase for the copolymer PVDF-TrFE (45/55 molar ratio) upon heating across its Curie temperature T_C using high temperature Quasielastic Neutron Scattering (QENS) and X-ray diffraction experiments. The β -to- α phase transition is observed to proceed in two stages with energetically distinct processes, which are identified as the nucleation of an intermediate phase with skew linkages and its subsequent transformation to the non-polar α phase. This

mechanism is similar to what is proposed for the reverse α -to- β transition, which also involves an intermediate phase to avoid pathways with large energy changes.^{20,23}

Polymer film samples of P(VDF-TrFE) (45/55 molar ratio) in their poled condition were purchased from Piezotech, S. A. S. (France). The thickness of the polymer films was 40 μm . The technical parameters are available from the supplier website and elsewhere.²⁷ The room temperature (RT) structural states of the poled PVDF-TrFE film was analyzed by scanning electron microscopy (SEM) and Fourier Transform Infrared (FTIR) spectroscopy. Scanning Electron Micrographs of cross-sections of the polymer films were obtained using JEOL JSM-6335F field-emission Scanning Electron Microscope. The cross-sections of the films were prepared carefully by cryo-fracture in a liquid nitrogen atmosphere. The prepared samples were coated with gold by sputtering. FTIR measurements were obtained at room temperature using a Perkin Elmer 1600 FTIR Spectrometer using a MIRacle, Single Reflection Horizontal ATR Accessory (Pike Technologies, USA). Figure 1(a,b) shows the scanning electron micrographs of the film, which contains a dispersion of disc-shaped particles in addition to regions with elongated strands. The stretching of the polymeric chains, as observed within the elongated strands, can induce transformation from the non-polar α phase to the polar β phase. The molecular configurations of the polymeric chains in the unpoled and poled films were obtained from the FTIR spectra,²⁸ as shown in Figure 1(c). The peaks corresponding to the $T_m > 4$ (all-trans), the TTTG (trans-trans-trans-gauche) and the TG (trans-gauche) bonds are marked in the plot. While the film shows strong peaks corresponding to the $T_{m>4}$ and the TTTG (trans-trans-trans-gauche) configurations, the peak for TG (trans-gauche) configuration is not noticeable.

The macroscopic phase transition behavior of the poled P(VDF-TrFE) film was characterized using dielectric permittivity and differential scanning calorimetry (DSC) measurements. The polymer films were coated with gold electrodes and contacted with electrical wires for dielectric measurements. The dielectric properties were measured in the frequency range from 100 Hz to 100kHz using an Agilent 4284A Precision LCR meter. All measurements were taken using an AC test voltage of 100 mV, while heating up from 200 K to 370 K. The results are shown in Figure 2(a). A sharp increase in the dielectric permittivity ϵ' is observed for temperatures 320 K and above, which can be associated with ferroelectric-to-paraelectric phase transition. Additionally, a broad shoulder is observed at $T \sim 250-300$ K, which is also frequency dispersive as indicated from the $\tan \delta$ spectra and indicates a relaxing transition within this temperature range. In our earlier study, we determined that a broad frequency-dispersive transition in PVDF copolymers can be associated with relaxational mechanisms at interfaces between crystalline and amorphous regions.²⁹ Here, our main focus lies on exploring the ferroelectric phase transition observed for temperature above 320 K. The thermal changes during the ferroelectric phase transition are probed by DSC. These measurements were carried out using a DSC 2910 Differential Scanning Calorimeter (TA Instruments) in nitrogen atmosphere, while heating the polymer samples from low temperature. The results are shown in Figure 2(b). Interestingly, the phase transition is observed to proceed in two stages. The first stage commences at ~ 310 K, while the second stage commences at ~ 325 K and the peak for the second stage is observed slightly below 340 K. In order to understand the physical mechanisms involving the two-

stages phase transition, we undertook detailed *in situ* QENS and XRD analyses of the polymer films at high temperatures.

The microscopic dynamics in the poled PVDF-TrFE polymer film was studied from QENS measurements using the backscattering spectrometer BASIS at the Spallation Neutron Source (SNS) of the Oak Ridge National Laboratory (ORNL).³⁰ QENS data were collected at standard instrument configuration that provides the dynamics range of $\pm 100 \mu\text{eV}$ energy transfer with an overall energy resolution of $3.4 \mu\text{eV}$ (full width at half-maximum, fwhm, Q-averaged value). QENS spectra from poled PVDF-TrFE at all measured temperatures were transformed to the dynamic susceptibility (imaginary part), $\chi''(Q, E) = \frac{S(Q, E)}{n_B(E)}$, where $S(Q, E)$ is the measured dynamics structure factor and $n_B(E)$ is Bose occupation factor, $n_B(E) \approx k_B T / E$. The dynamic susceptibility shows distinct peaks at different energy transfers as a signature of multiple dynamics processes occurring at corresponding energy regimes. Presence of at least two peaks in the dynamic susceptibility of poled PVDF-TrFE (Figure 3(a)), at lower and higher energy transfers can be noticed, which reveals the different microscopic dynamic processes occurring over the temperature range for β -to- α phase transition. Furthermore, as is clearly revealed from Figure 3(b), the higher energy transfer peak is characterized by a Q-independent position, but has strongly Q-dependent intensity, which indicates a more localized relaxation of the polymer molecules. At the same time, the position of the lower energy transfer peak is comparatively more Q-dependent, which suggests the less spatially localized motion of this process as compared to the one at higher energies.

In order to understand the crystallographic and mesoscopic structural changes which could be related to the two different stages and the two different energy processes during the β -to- α phase transition, we undertook *in situ* high-temperature XRD experiments of the polymer film. The polymer sample in the form of a foil was examined with aid of Bruker D8 Advance XRD equipped with an Anton Paar high temperature attachment model HTK-1200N and high speed PSD detector model Vantec-1. The X-ray beam was produced using a Cu anode X-ray tube and shaped by a Göbel Mirror and 0.6 mm incident beam aperture. The sample was placed on a zero background sample holder made from single crystal sapphire and measured over the angular 2θ range of $5-50^\circ$ with a scan rate $1.5^\circ/\text{min}$. All measurement temperatures were reached with heating rate $30^\circ\text{C}/\text{min}$ and calibrated using the known solid-solid phase transitions of several standards.

Figure 4(a) shows the evolution of the diffraction patterns as a function of temperature in the 2θ range of $17^\circ-20^\circ$, which shows the major crystalline peaks from the ferroelectric and the paraelectric phases. The peak at $2\theta \sim 19.3^\circ$ observed at room temperature (RT) can be attributed to the 200 and 110 diffraction peaks from the ferroelectric β phase, which has all-T configuration.³¹ In addition to the main diffraction peak, a shoulder centered at $2\theta \sim 19^\circ$ can be observed. This second peak is attributed to γ phase that is intermediate between the ferroelectric and the paraelectric phases and has a majority of T bonds over the G bonds.³¹ The identification of the phases from XRD at RT is consistent with peaks observed in the FTIR pattern as shown in Figure 1(c). With increasing temperature, the median of the diffraction pattern shifts to lower angles. At higher temperatures, the center of the peak at $2\theta \sim 18^\circ$ can be attributed to

the α phase. Interestingly, the β -to- α transition does not occur abruptly but through gradual evolution over a range of temperatures. This conclusion is corroborated by gradual rather than abrupt evolution with temperature of the dynamic susceptibility spectra presented in Figure 3.

In order to understand the crystallographic changes over the measured temperature range for β -to- α transition, the diffraction patterns at each temperature is fitted with Gaussian peak profile functions. The XRD patterns for temperatures up to $T = 340$ K are fitted with two crystalline peaks corresponding to the β and γ phases, in addition to a broad background corresponding to the amorphous phase, as illustrated in Figure 4(b). The 110 and 200 reflections could not be distinguished from the measured peak profiles, and therefore a single peak was used to account for both of these reflections from each of the two phases. The corresponding lattice parameters calculated from the peak fitting procedure are shown in Figure 4(c). The lattice spacing for the α phase increases linearly up to $T = 340$ K, beyond which the (110)/(200) reflection from this phase disappears. However, the lattice spacing of the γ phase shows a non-linear temperature-dependent increase beginning at $T \sim 318$ K. Still, a continuous transition to higher lattice spacings for the γ phase can be observed up to $T = 340$ K, beyond which the peak merges with the 100 reflection of the paraelectric α phase. These observations therefore indicate that concurrent with a steady depletion of the ferroelectric β phase, there are changes in the γ phase as well.

In order to further understand the mesoscopic evolution of the different phases with temperature, we analyzed the intensity ratios and widths of the diffraction peaks, which are shown in Figure 4(d). The intensity of a diffraction peak from a particular

phase indicates its relative abundance in the microstructure. As shown in the top panel of Figure 4(d), the relative intensity of the (110)/(200) reflection from the β phase continues to decrease with increasing temperature above $T = 310$ K. The rate of decrease is more gradual between 310 and 325 K, beyond which it accelerates and eventually the peak disappears at $T = 345$ K. These two stages for decrease of $I(\beta)$ matches exactly with the two stages observed from the DSC plot, which is superimposed on Figure 4(d), thereby partially clarifying the phase transition mechanism.

The lower panel of Figure 4(d) shows the widths of the diffraction peaks originating from β and γ phases as a function of temperature. The change in the width of a diffraction peak, other factors remaining the same, is inversely proportional to the change in particle or domain sizes of the corresponding crystalline phase. Using Scherrer's equation, the average particle size of the β phase is estimated ~ 20 nm, whereas the same for the γ phase is ~ 10 nm. Although these estimates are somewhat compromised by the elongated nature of some of particles, especially for the β phase, they are more or less consistent with visual observation of Figure 1(a). With increase in temperature, we first observe an increase in diffraction peak width for the γ phase, which is consistent with the first stage observed in the DSC plot for $T < 325$ K. The peak width for the γ phase subsequently decreases in the second stage. A gradual increase in the peak width for the β phase is observed for $T > 325$ K, which is also consistent with accelerated decrease in its peak intensity observed during the second stage of DSC plot.

Following the above observations, we propose the following pathway for β -to- α phase transition. At RT, the poled polymer film has coexisting particles of β and γ phases, which correspond to bond configurations of all-T and TTTG, respectively. In the first stage of the phase transition, beginning at $T \sim 310$ K, nucleation of additional γ phase occurs from the existing β phase particles. This is reflected in a small decrease in the (110)/(200) peak intensity of the β phase. Since, the nucleated particles of an additional γ phase are smaller in size than the existing low-temperature γ phase particles, the average peak width for this phase shows an increase in size during this stage. Additionally, we observe a non-linear increase in the average lattice parameter obtained from the (110)/(200) reflection of the γ phase, which indicates that the lattice parameters of the γ phase particles nucleated at this stage should be larger than the existing low-temperature γ phase. This can be justified based on the fact that the nucleated γ phase does not have a regular TTTG configuration, but a random distribution of skew linkages in between *trans* segments.³¹ In the second stage of the phase transition, the γ phase particles grow at the expense of the remaining β particles. This is reflected in the decrease in peak width for the γ phase and a simultaneous increase in the peak width for the β phase - these are concurrent with accelerated decrease in diffraction peak intensity from β phase. Finally, the γ phase transforms to α phase, as can be observed from merging of the (110)/(200) reflection of the γ phase into the (100) reflection of the α phase.

The sequence of structural transformations proposed above can be understood in terms of recent predictions from first-principles calculations.^{20,23} It was hypothesized that since a direct α - β transformation pathway requires much higher energies, the

ferroelectric-paraelectric phase transition should instead proceed through an intermediate phase. We show here that the β -to- α phase transition indeed proceeds through an intermediate γ phase. The conversion of β to γ involves torsion along the C-chain and therefore is energetically more intensive. At higher temperatures, the lattice parameter of the γ phase approaches that of the α phase and then the γ -to- α transformation can simply be achieved by 180° rotation of some of the polymer chains – this process is less energy intensive than the former. This can explain why the final transformation from γ -to- α does not significantly contribute to exotherm in the DSC plot. The proposed phase transformation mechanism in poled PVDF-TrFE polymer, which occur at different energy scales, are well captured in the dynamic susceptibility data presented in Figure 3. The peak at lower energy transfer, which is also relatively more prominent at smaller Q, is likely associated with the local transitional mobility of the polymer chains as a result of 180° flipping on transforming from γ to α phase. Since the low energy peak position changes with an increase in temperature, it suggests that polymer chains become more isolated to reorient for a complete conversion from γ to α phase. The high energy peak can be assigned to the torsion of polymer molecules along C-C chain that occurs during the conversion of β to γ phases. Furthermore, evolution of high energy transfer peaks also shows growing prominence of the localized relaxations with increasing temperatures.

Finally, Figure 5 compares the diffraction peak profiles of a poled film with that of the same film after thermal cycling above T_C . It can be observed that while there is partial conversion from α to γ upon cooling, the β phase is not recovered at all. This clearly shows that the 180° rotation of the polymer chains is partially reversible with

thermal cycling, while the β -to- γ process is not. This can again be understood as a result of lower energy barrier for the 180° flipping of the chains than that for torsion along the C-chains.²⁰ Such irreversible phase transition behavior explains the depoling behavior of PVDF copolymer films with all-T configuration at high temperatures. It can also lower the efficiency of these materials for electrocaloric applications, which requires interconversion between ferroelectric and paraelectric phases.¹⁰ However, as shown earlier, the driving force for conversion from γ to β is mechanical torsion.²⁰ Since γ phase is recoverable from α after thermal cycling, it could be possible to achieve repeatable transformation between β and α phases by operating under an appropriate mechanical stress. Such stress could be applied externally or introduced through microstructural means such as introduction of secondary phase in composites. These means could be explored to improve the thermal stability and/or electrocaloric efficiency of PVDF copolymer films.

In summary, we undertook direct experimental investigations of the crystallographic and mesoscopic mechanisms for ferroelectric β to paraelectric α phase transition in poled PVDF-TrFE copolymer films using a combination of *in situ* XRD and QENS measurements at high temperatures. The β -to- α phase transition proceeds through an intermediate γ phase with random skew linkages between the trans segments. Furthermore, it is shown that the phase transition proceeds in two stages via two different energy processes, which are identified here as the nucleation and growth of new γ phase particles from β and conversion of γ to α . The conversion of γ to α is an energetically less intensive process and do not significantly add to heat flow during the

ferroelectric-paraelectric phase transition. Possible means to achieve repeatability for transformations between ferroelectric and paraelectric phase are discussed.

Acknowledgements

AP gratefully acknowledges funding support from CityU (Project Numbers 7200514 and 9610377). The experiments conducted at the Spallation Neutron Source (SNS), High Flux Isotope Reactor (HFIR) and Center for Nanophase Materials Sciences (CNMS) in Oak Ridge National Laboratory was supported by the Scientific User Facilities Division, Office of Basis Energy Sciences, U. S. Department of Energy. STM thanks his Inamori Professorship which supported the HTXRD work at Alfred University. AP gratefully acknowledges technical assistance from Mr. Daniel Yau, Mr. Tak Fu Hung and Mr. Tit Wah Chan.

References:

1. H. Kawai, Japan. J. Appl. Phys. **8**, 975-976 (1969)
2. T. Furukawa, M. Date, E. Fukada, Y. Tajitsu and A. Chiba, Japan. J. Appl. Phys. **19**, L109-L112 (1969)
3. A. L. Lovinger, Science **220**, 1115-1121 (1983)
4. A. V. Bune, V. M. Fridkin, S. Ducharme, L. M. Blinov, S. P. Palto, A. V. Sorokin, S. G. Yudin and A. Zlatkin, Nature **391**, 874-877 (1998)
5. Q. M. Zhang, V. Bharti and X. Zhao, Science **280**, 2101-2104 (1998)
6. M. Li, H. J. Wondergem, M.-J. Spijkman, K. Asadi, I. Katsouras, P. W. M. Blom and D. M. de Leeuw, Nat. Mater. **12**, 433-438 (2013)
7. F. Bauer, Appl. Phys. A **107**, 567-573 (2012)
8. M. Li, I. Katsouras, C. Piliego, G. Glasser, I. Lieberwirth, P. W. M. Blom and D. M. de Leeuw, J. Mater. Chem. C **1**, 7695-7702 (2013)
9. B. Chu, X. Zhou, K. Ren, B. Neese, M. Lin, Q. Wang, F. Bauer and Q. M. Zhang, Science **313**, 334-336 (2006) (energy storage)
10. X. Moya, S. Kar-Narayan and N. D. Mathur, Nat. Mater. **13**, 439-450 (2014)
11. C. Wan and C. R. Bowen, J. Mater. Chem. A **5**, 3091-3128 (2017) (energy harvesting)
12. X. Chen, X. Han and Q.-D. Shen, Adv. Electron. Mater. 1600460 (2017)
13. M. Bohlen and K. Bolton, Phys. Chem. Chem. Phys. **16**, 12929-12939 (2014)
14. Z. Cui, N. T. Hassankiadeh, Y. Zhuang, E. Drioli and Y. M. Lee, Progress in Polymer Science **51**, 94-126 (2015)

15. M. E. Lines and A. M. Glass, *Principles and Applications of Ferroelectrics and Related Materials* (Clarendon Press, Oxford, 1977)
16. R. A. Cowley and S. M. Shapiro, *J. Phys. Soc. Jpn.* **75**, 111001 (2006)
17. Y. Abe, K. Tashiro, M. Kobayashi, *Computational and Theoretical Polymer Science* **10**, 323-333 (2000)
18. Y. Abe and K. Tashiro, *J. Poly. Sci. B: Pol. Phys.* **39**, 689-702 (2001)
19. W. J. Heo, W.-J. Kim, Y.-H. Shin and E. K. Lee, *Phys. Status Solidi RRL* **6**, 217-219 (2012)
20. V. Ranjan, M. Buongiorno Nardelli and J. Bernholc, *Phys. Rev. Lett.* **108**, 087802 (2012)
21. L. Li, M. Zhang, M. Rong and W. Ruan, *RSC Adv.* **4**, 3938-3943 (2014)
22. C. M. Hess, A. R. Rudolph and P. J. Reid, *J. Phys. Chem. B* **119**, 4127-4132 (2015)
23. W. J. Kim, M. H. Han, Y.-H. Shin, H. Kim and E. K. Lee, *J. Phys. Chem. B* **120**, 3240-3249 (2016)
24. P. Sajkiewicz, A. Wasiak and Z. Goclowski, *Eur. Pol. J.* **35**, 423-429 (1999)
25. T. Furukawa, T. Nakajima and Y. Takahashi, *IEEE Trans. Dielectrics and Electrical Insulation* **13**, 1120-1131 (2006)
26. V. Sencadas, R. Gregorio Jr. and S. Lanceros-Mendez, *J. Macromolecular Sci. Part B: Physics* **48**, 514-525 (2009)
27. N. Jalarvo, A. Pramanick, C. Do and S. O. Diallo, *Appl. Phys. Lett.* **107**, 082907 (2015)

28. M. R. Gadinski, Q. Li, G. Zhang, X. Zhang and Q. Wang, *Macromolecules* **48**, 2731-2739 (2015)
29. A. Pramanick, N. C. Osti, N. Jalarvo, S. T. Misture, S. O. Diallo, E. Mamontov, Y. Luo, J.-K. Keum and K. Littrel, unpublished
30. E. Mamontov and K. W. Herwig, *Rev. Sci. Instrum.* **82**, 085109 (2011)
31. K. Tashiro, K. Takano, M. Kobayashi, Y. Chatani and H. Tadokoro, *Polymer* **25**, 195-208 (1984)

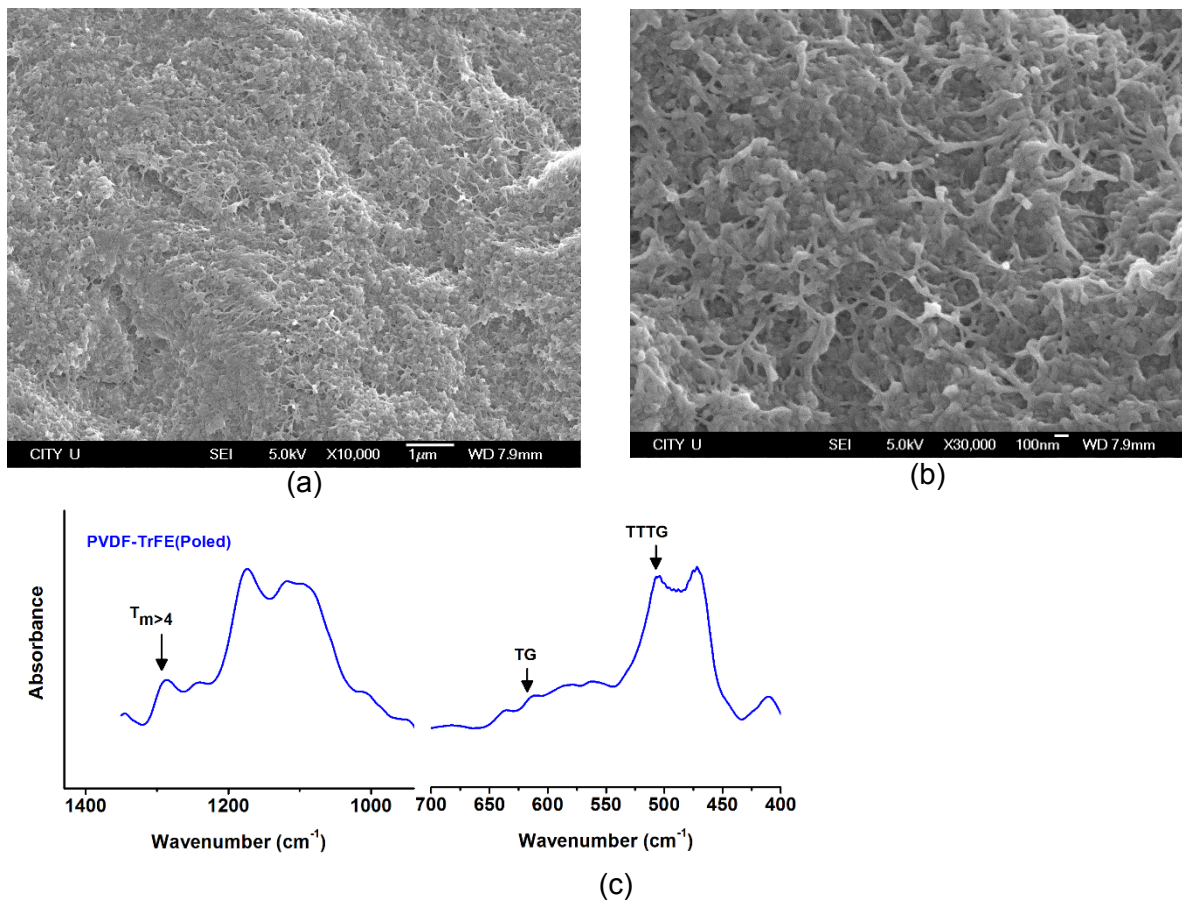
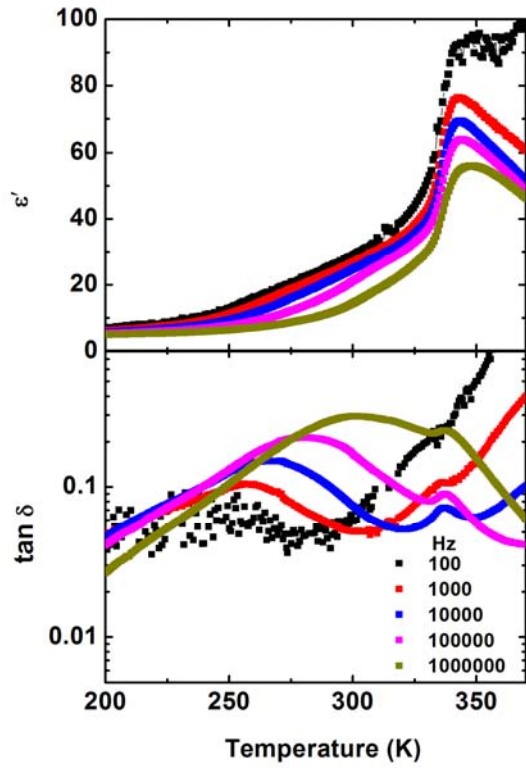
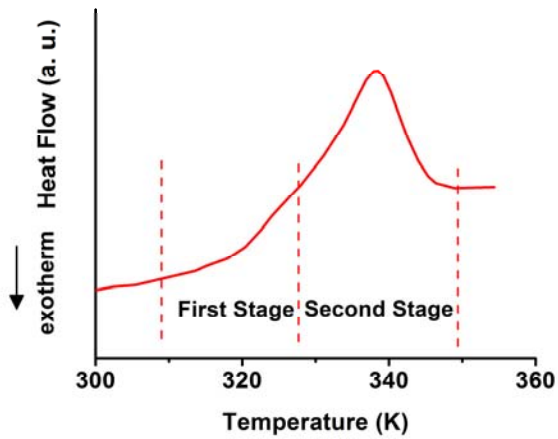


Figure 1: (a,b) Scanning electron micrographs of cross-sections of the poled PVDF-TrFE copolymer film. A high-magnification view shows presence of both elongated strands and disc-like particles. (c) FTIR spectra of the poled film showing the relative presence of the molecular configurations corresponding to the different crystalline phases at room temperature.

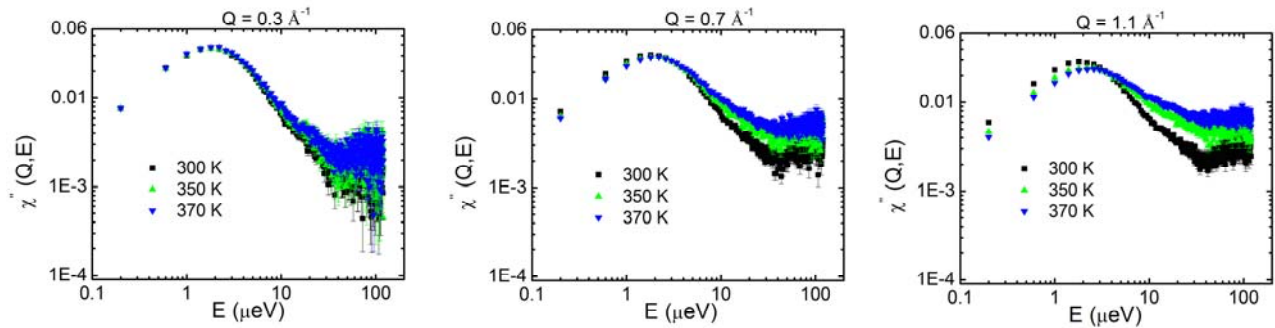


(a)

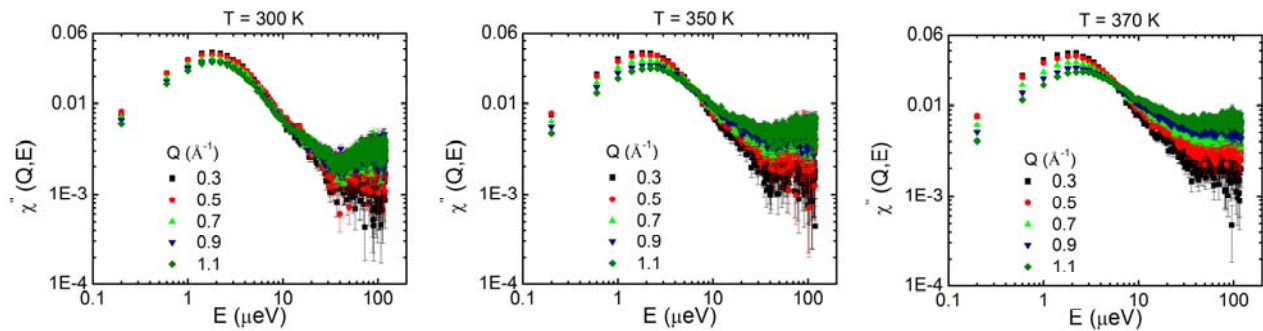


(b)

Figure 2: (a) Real (ϵ') component of the dielectric permittivity and loss $\tan \delta$ of poled PVDF-TrFE copolymer film. (b) DSC thermogram showing two stages for the ferroelectric-to-paraelectric phase transition.



(a)



(b)

Figure 3: Dynamic susceptibility from QENS data collected from poled PVDF-TrFE sample (a) QENS data at three representative Q values at indicated temperatures showing distinct relaxation processes at different energy transfers. (b) Q dependence of dynamic susceptibility at three different temperatures. The peak at higher energy transfers is characterized by Q -independent position but strongly Q -dependent intensity, while the lower energy-transfer peak is comparatively more Q -dependent.

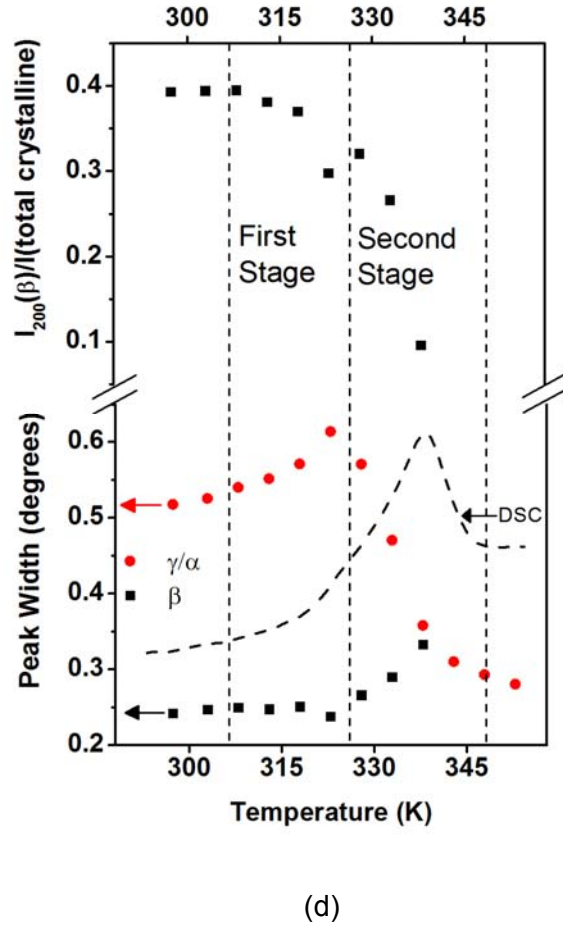
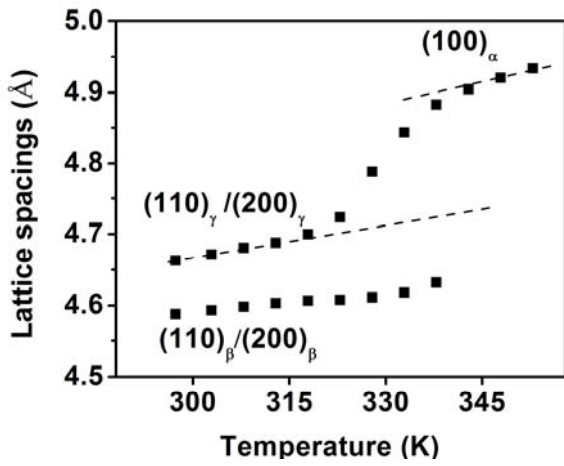
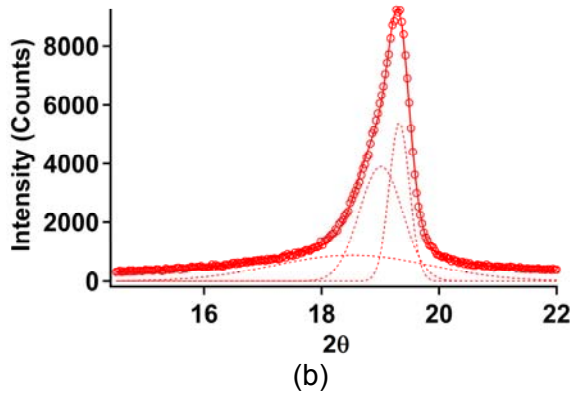
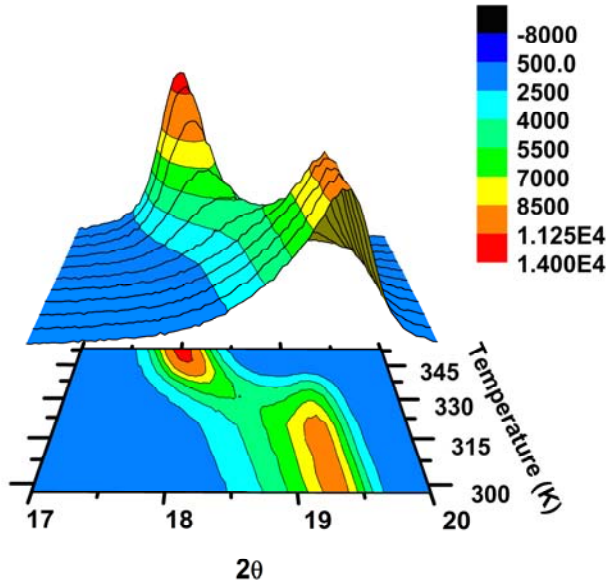


Figure 4: (a) High-temperature X-ray diffraction patterns from poled PVDF-TrFE copolymer film (b) Representative fit of X-ray diffraction peak for the poled PVDF-TrFE polymer film measured at 300 K. The peak profile is fit with three Pearson VII functions, which account for the two peaks from crystalline phases and a broad background from an amorphous phase. (c) Evolution of lattice parameters as function of temperature, which was obtained from fitting of the X-ray diffraction peaks. (d) The mesoscopic structural mechanisms during the ferroelectric-paraelectric phase transition are revealed from temperature-dependent peak intensities and peak widths, as shown in the top and bottom panels, respectively. The DSC curve is also superimposed with a dotted line, in order to illustrate how the microstructural changes correlate to thermal changes during the phase transition.

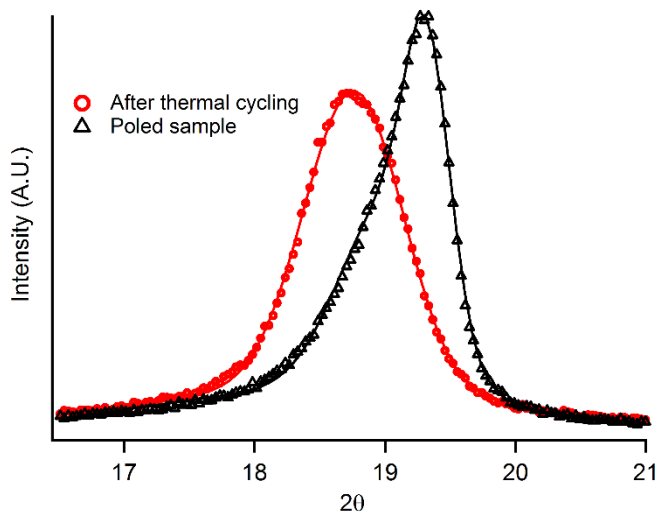


Figure 5: X-ray diffraction profiles of the polymer films in poled condition and upon thermal cycling.